Comparison of Different Modes of Two-Dimensional Reverse-Correlation NMR for the Study of Proteins

AD BAX,* MITSUHIKO IKURA,* LEWIS E. KAY,* DENNIS A. TORCHIA†
AND ROLF TSCHUDIN*

*Laboratory of Chemical Physics, National Institute of Diabetes and Digestive and Kidney Diseases, and
† Bone Research Branch, National Institute of Dental Research, National Institutes of Health,
Bethesda, Maryland 20892

Different two-dimensional NMR schemes for generating ^{1}H-detected ^{1}H–^{15}N and ^{1}H–^{13}C correlation spectra are compared. It is shown that the resolution in the dimension that represents the ^{13}C or ^{15}N chemical shift depends on the type of correlation scheme used. For ^{15}N NMR studies of proteins, it is found that experiments that involve ^{15}N single-quantum coherence offer improved resolution compared to multiple-quantum correlation experiments, mainly because the ^{1}H–^{1}H dipolar broadening of the multiple-quantum coherence is stronger than the heteronuclear dipolar broadening of ^{15}N, but also because of the presence of unresolved J splittings in the F_1 dimension of the multiple-quantum correlation spectra. For ^{13}C, the heteronuclear dipolar interaction is much larger and the ^{1}H–^{13}C multiple-quantum relaxation is slower than the ^{13}C transverse relaxation; however, because of the presence of ^{1}H–^{1}H J couplings in the F_1 dimension of such spectra, in practice the multiple-quantum type correlation experiments often offer no gain or even a small loss in resolution, compared to experiments that use transverse ^{13}C magnetization during the evolution period. A modified pulse scheme that increases F_1 resolution by elimination of scalar relaxation of the second kind is proposed. Experiments for the proteins calmodulin, uniformly enriched with ^{15}N, and staphylococcal nuclease, labeled with ^{13}C in the Cα position of all Pro residues are demonstrated.
© 1990 Academic Press, Inc.

Two-dimensional ^{1}H-detected heteronuclear chemical-shift correlation schemes (1–7) offer a large increase in sensitivity over the older 2D correlation experiment that relies on direct detection of the nucleus with the low magnetogyric ratio, γ (8–10). Either at natural abundance (11–13) or with isotopic enrichment (14–18), the new methods can provide useful additional assignment information for proteins of up to several hundred amino acids. The ^{1}H-detected experiments are often referred to as reverse correlation experiments. The large number of different pulse sequences proposed for reverse correlation basically can be divided into two types: experiments that utilize heteronuclear multiple-quantum coherence during the evolution period, t_1, and experiments that rely on low-γ transverse magnetization during t_1. The heteronuclear multiple-quantum experiments are all derivatives of experiments proposed originally by Müller (1). Most of the ^{1}H-detected single-quantum correlation experiments are variations on an experiment first proposed by Bodenhausen and Ruben (2). This experiment employs two INEPT type transfers (19) to transfer magnetiza-

tion from the protons to the low-γ nucleus and back to the protons. The enhancement in sensitivity possible with this scheme dwarfs the enhancement obtainable with the nuclear Overhauser effect (when observing the low-γ nucleus directly), and therefore it has been referred to as the Overbodenhausen experiment (4, 20). Below, the advantages and disadvantages of multiple-quantum vs single-quantum correlation experiments will be discussed, and a variation on the Overbodenhausen experiment that removes line broadening caused by scalar relaxation of the second kind is described (21).

Two types of broadening are present in the reverse correlation experiments: homogeneous broadening due to relaxation and heterogeneous effects caused by unresolvable homonuclear and heteronuclear J couplings. The effects of these broadening mechanisms will be discussed for the four different pulse sequences, sketched in Fig. 1. Below, the magnetization transfer processes will be discussed in terms of the operator formalism (22), but for simplicity *only terms that contribute to the final spectrum are retained*. In this description, the effect of the pulse sequence between the end of the magnetization recovery period and the beginning of the evolution period is summarized by an operator A; the conversion between the end of the evolution period and the start of t_2 is described by B.

EXPERIMENTAL METHODS

The HMQC experiment. For a heteronuclear I–S system (I = ^{1}H, S = ^{13}C or ^{15}N) the scheme of Fig. 1a, often referred to as heteronuclear multiple-quantum correlation (HMQC) (23) or "forbidden echo" (6), can be described by

$$I_z \xrightarrow{A} -2I_xS_y \xrightarrow{t_1} -2I_xS_y\cos\,\Omega_St_1 \xrightarrow{B} -I_y\cos\,\Omega_St_1, \qquad [1]$$

where for simplicity the effect of ^{1}H chemical shift (refocused by the 180° ^{1}H pulse) has been omitted, and pulse phases corresponding to the first step of the phase cycle (Fig. 1) have been assumed. In this expression, Ω_S denotes the angular offset frequency of spin S. Expression [1] indicates that the detected in-phase ^{1}H signal (I_y) is modulated in amplitude by Ω_S, giving rise to a single absorptive correlation in the 2D spectrum.

Above, the presence of other protons that may be coupled to I or S has been neglected. Below, we will briefly consider the effect of a second proton, K. The extension to an arbitrary number of protons is then straightforward. For our purpose here, the effect of the relatively small homonuclear coupling J_{IK} during the short delays, Δ, may be neglected. During the evolution period, dephasing caused by any J_{SK} coupling is refocused by the 180° ^{1}H pulse. However, dephasing caused by J_{IK} coupling is not refocused since both spins I and K experience the effect of the nonselective 180° pulse. Consequently, the magnetization transfer process can be summarized by

$$I_z \xrightarrow{At_1B} -I_y\cos\,\pi J_{IK}t_1\cos\,\Omega_St_1 + 2I_xK_z\sin\,\pi J_{IK}t_1\cos\,\Omega_St_1. \qquad [2]$$

If the data are transformed using either the States (24) or the TPPI method (25), such a signal results in four multiplet components at ($\Omega_S \pm \pi J_{IK}$, $\Omega_I \pm \pi J_{IK}$). This multiplet contains in-phase absorptive components and antiphase dispersive compo-
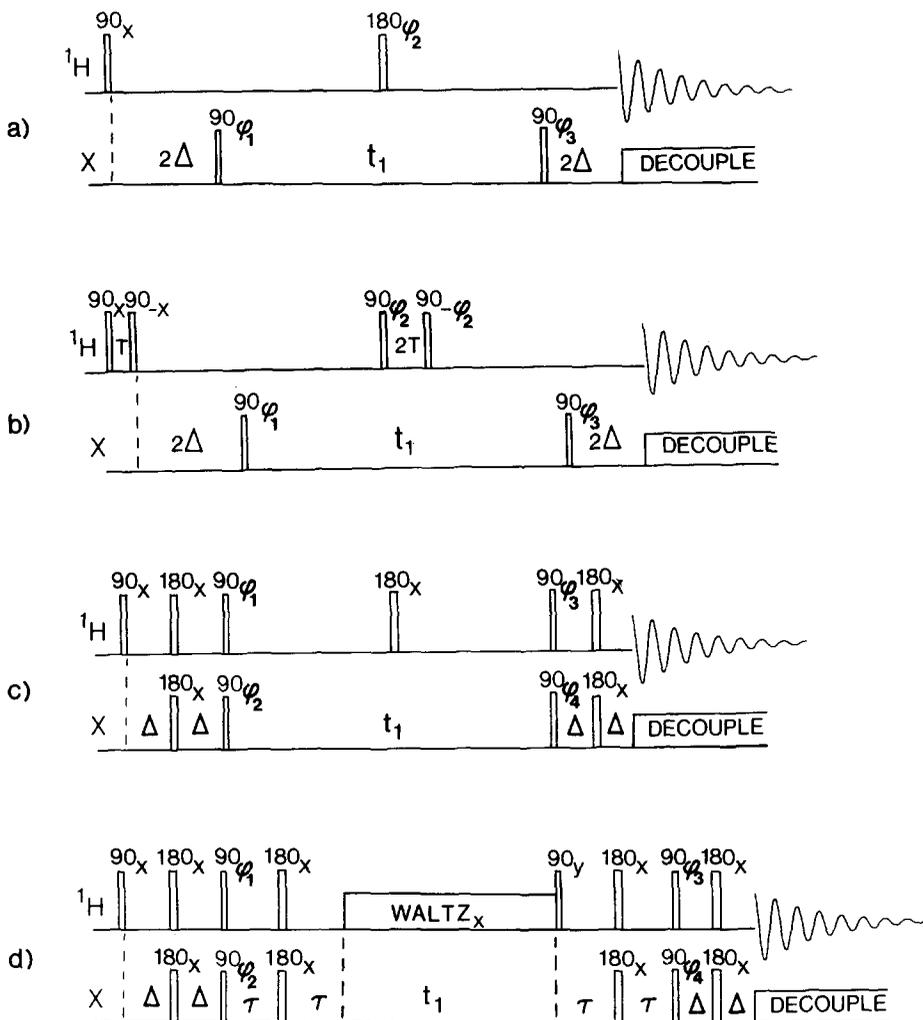
BAX ET AL.

FIG. 1. Schemes for ^{1}H-detected heteronuclear chemical-shift correlation. (a, b) The HMQC schemes utilizing heteronuclear multiple-quantum coherence during the evolution period. Scheme a requires pre-saturation of the solvent resonance when spectra are recorded in H_2O solution; scheme b utilizes jump-and-return pulses for suppression of the solvent resonance. (c, d) Two versions of the Overbodenhausen correlation experiment that utilize single-quantum X-nucleus coherence during the evolution period. Scheme c utilizes a 180° pulse for removing the net effect of heteronuclear coupling; scheme d uses a composite pulse decoupling scheme preceded by a refocusing interval, $2\tau = 1/(2J_{XH})$, and followed by a defocusing period of duration 2τ. The WALTZ decoupling sequence should always start at the same position in its cycle, and if all WALTZ pulses are applied along the x axis, a purge pulse applied immediately at the end of the t_1 period should be 90° out of phase relative to the WALTZ pulses. To minimize relaxation effects, for proteins the delay Δ is usually set to a value slightly ($\approx 20\%$) shorter than $1/(4J_{XH})$. For sequence b, the delay T is set to $1/(4\delta)$, where δ is the offset at which maximum excitation is desired, and the carrier is positioned on the H_2O resonance. The phase cycling used for schemes a and b is $\phi_1 = x, -x$; $\phi_2 = x, x, y, y, -x, -x, -y, -y$; Acq. $= 2(x, -x, -x, x)$; to suppress incomplete steady-state effects during the pulse sequence (38), ϕ_3 is inverted after 8 scans (from x to $-x$) and the receiver phase is inverted, too. For schemes c, d; $\phi_1 = y, -y$; $\phi_2 = 2(x), 2(-x)$; $\phi_3 = 4(x), 4(-x)$; Acq. $= x, -x,$ $-x, x, 2(-x, x, x, -x), x, -x, -x, x$; $\phi_4 = 8(x), 8(-x)$. After 16 scans, the phase of the first 180° (X) pulse following the evolution period in scheme d is inverted, without changing the receiver phase. This pulse is the only composite pulse ($90^\circ_x 180^\circ_y 90^\circ_x$) used.

nents (*26*). The main point we wish to draw attention to, however, is that the correlation shows homonuclear J coupling structure in the F_1 dimension.

The linewidth in the F_1 dimension is determined by the relaxation rate of the multiple-quantum coherence, $I_x S_y$ (*26, 27*). The antiphase term $I_y S_y K_z$ (present during the t_1 period) relaxes slightly faster because of the finite lifetime of K_z, but this small increase will not be considered here. Neglecting K–S dipolar coupling, cross correlation and chemical-shift anisotropy, the transverse relaxation rates of the I-spin, S-spin, and multiple-quantum coherence are given by

$$1/T_{2I} = \tfrac{1}{20}D_{IS}^2[4J(0) + J(\omega_I - \omega_S) + 3J(\omega_I) + 6J(\omega_S) + 6J(\omega_I + \omega_S)]$$

$$+ \tfrac{1}{20}\sum_K D_{IK}^2[5J(0) + 9J(\omega_I) + 6J(2\omega_I)] \quad [2a]$$

$$1/T_{2S} = \tfrac{1}{20}D_{IS}^2[4J(0) + J(\omega_I - \omega_S) + 3J(\omega_S) + 6J(\omega_I) + 6J(\omega_I + \omega_S)] \quad [2b]$$

$$1/T_{2MQ} = \tfrac{1}{20}D_{IS}^2[J(\omega_I - \omega_S) + 3J(\omega_I) + 3J(\omega_S) + 6J(\omega_I + \omega_S)]$$

$$+ \tfrac{1}{20}\sum_K D_{IK}^2[5J(0) + 9J(\omega_I) + 6J(2\omega_I)], \quad [2c]$$

where $J(\omega) = \tau_c/(1 + \omega^2\tau_c^2)$ and τ_c is the correlation time. Other constants are $D_{IS} = h\gamma_I\gamma_S/(2\pi r_{IS}^3)$, h is Planck's constant, γ_I and γ_S are the magnetogyric ratios of spin I and S, respectively, and r_{IS} is the I–S internuclear distance. The constant D_{IK} refers to the homonuclear dipolar interaction between spin I and spin K; $D_{IK} = h\gamma_I^2/(2\pi r_{IK}^3)$. For proteins at field strengths above 10 T, with I = ^{1}H and S = ^{13}C or ^{15}N, all spectral density terms except for $J(0)$ and $J(\omega_S)$ are extremely small and may be safely ignored, yielding

$$1/T_{2I} = \tfrac{1}{10}D_{IS}^2[2J(0) + 3J(\omega_S)] + \tfrac{1}{4}J(0)\sum_K D_{IK}^2 \quad [3a]$$

$$1/T_{2S} = \tfrac{1}{20}D_{IS}^2[4J(0) + 3J(\omega_S)] \quad [3b]$$

$$1/T_{2MQ} = \tfrac{1}{4}J(0)\sum_K D_{IK}^2 + 3/20J(\omega_S)D_{IS}^2. \quad [3c]$$

As shown previously for ^{15}N, the effect of the heteronuclear dipolar coupling on the transverse relaxation of amide protons in proteins is significant and therefore T_{2MQ} is often longer than T_{2H}, the transverse relaxation time of a proton attached to ^{14}N or ^{15}N (*27*). For ^{13}C, the heteronuclear dipolar coupling to a directly attached proton is about a factor of two larger than for ^{15}N, and usually it is the dominant transverse relaxation mechanism both for ^{13}C and for the proton attached to ^{13}C. (For methylene sites, the strong homonuclear dipolar coupling is of the same magnitude as the ^{1}H–^{13}C coupling.) Consequently, the relaxation time of ^{1}H–^{13}C multiple-quantum coherence is expected to be longer than the T_2 of ^{13}C or protons attached to ^{13}C, and nearly identical to the T_2 of protons attached to ^{12}C.

The jump-and-return HMQC sequence. A jump-and-return version of the HMQC sequence was first used by Roy *et al.* (*6*). At first sight, the only difference from the sequence of Fig. 1a is that no presaturation of the H$_2$O resonance is needed and that the jump-and-return type pulses introduce a $\sin^3(2\pi\delta T)$ intensity dependence in the

F_2 dimension (28), where δ is the offset from the H_2O frequency and T is the delay in the 1–1 sequence. However, an additional difference with the scheme of Fig. 1a occurs because $C\alpha H$ protons typically resonate in the vicinity of the H_2O resonance and they are not inverted by the 90°_ϕ–2τ–$90^\circ_{-\phi}$ sequence applied at the midpoint of the evolution period. Hence, the effect of homonuclear coupling with the NH protons is refocused and no homonuclear J modulation occurs. In contrast, heteronuclear long-range couplings between ^{15}N and $C\alpha H$ and $C\beta H$ protons, which are not inverted by the 90°_ϕ–2τ–$90^\circ_{-\phi}$ sequence, remain. The relevant terms during the magnetization transfer process are summarized by

$$I_z \xrightarrow{\quad At_1 \quad} -2I_xS_y\cos \Omega_St_1\cos \pi J_{NK}t_1 \xrightarrow{\quad B \quad} -I_y\cos \Omega_St_1\cos \pi J_{NK}t_1. \quad [4]$$

This expression shows that a purely absorptive 2D signal is obtained. However, the F_1 resolution is affected by usually unresolvable J couplings, J_{NK}, between the ^{15}N and the $C\alpha H$ (and $C\beta H$) protons that resonate in the vicinity of the H_2O frequency. Of course, the transverse relaxation rate of the mutiple-quantum coherence is identical to the rate for the regular HMQC scheme. As demonstrated later, the F_1 resolution in the 2D spectrum can be substantially different for the two methods.

The Overbodenhausen experiment. The pulse scheme originally proposed by Bodenhausen and Ruben (2) employs an INEPT sequence (19) to transfer ^1H magnetization I_z into antiphase ^{15}N magnetization. ^1H decoupling during the evolution period is accomplished in the standard manner by the application of a 180° ^1H pulse at the midpoint of t_1 (8). A subsequent INEPT transfer reconverts the transverse ^{15}N magnetization into observable ^1H magnetization. The whole process is summarized by

$$I_z \xrightarrow{\quad \text{INEPT} \quad} -2I_zS_y \xrightarrow{\quad t_1 \quad} -2I_zS_y\cos \Omega_St_1 \xrightarrow{\quad \text{reverse INEPT} \quad} -I_x\cos \Omega_St_1.$$

$$[5]$$

Expression [5] indicates that pure absorptive lineshapes can be obtained. The F_1 linewidth is not affected by ^1H–^1H or ^1H–^{15}N J couplings and, neglecting static field inhomogeneity, it is solely determined by the average relaxation rate of S_x and I_zS_y. The transverse relaxation rate of I_zS_y corresponds to the sum of the rate of decay of S_y (which is the reciprocal of the ^{15}N T_2) and the longitudinal relaxation rate of I_z. This latter contribution can be considered scalar relaxation of the second kind (21); whenever I_z changes its spin state, the ^{15}N doublet component changes its frequency by J_{NH}. Therefore, the F_1 linewidth corresponds to the ^{15}N linewidth in a ^1H-coupled ^{15}N spectrum. As will be discussed later, narrower lines, without the scalar relaxation broadening, can be obtained with the pulse scheme of Fig. 1d.

In the Overbodenhausen experiment, neglecting relaxation, all ^1H magnetization is transferred into antiphase S-spin magnetization and this antiphase S-spin magnetization is transferred back into ^1H magnetization at the end of the evolution period. The efficiency of magnetization transfer is independent of the multiplicity, n, of the I_nS moiety. Therefore, in contrast to the refocused version of the Overbodenhausen experiment discussed below, no magnetization loss occurs for these groups.

The decoupled Overbodenhausen experiment. The scalar relaxation contribution to the F_1 linewidth in spectra recorded with the scheme of Fig. 1c can be removed by recording the spectrum with continuous decoupling during the evolution period, as indicated in Fig. 1d. This not only enhances the resolution in the 2D correlation map but it also makes it possible to measure ^{13}C or ^{15}N T_2 values directly from a single spectrum, providing valuable information on local protein dynamics.

The scheme of Fig. 1d utilizes refocused INEPT transfer (*29, 30*) to generate in-phase S-spin magnetization. Decoupling used during t_1 is of the composite pulse type to minimize any broadening resulting from residual scalar interactions. One point regarding this decoupling requires special attention: since decoupling is applied on the ^{1}H channel, and signals from protons not coupled to the heteronucleus are to be canceled by subtracting the results from consecutive scans with opposite S-spin RF pulse phase, it is important that the decoupling sequence applied in consecutive scans be exactly the same. In other words, it is essential to start the decoupling sequence always at the same position within a composite pulse decoupling cycle; i.e., the composite pulse decoupling should be running in a synchronous manner.

The magnetization transfer during the sequence of Fig. 1d can again be summarized as

$$I_z \xrightarrow{\text{INEPT}} S_x \xrightarrow{t_1} S_x \cos \Omega_S t_1 \xrightarrow{\text{reverse INEPT}} I_x \cos \Omega_S t_1, \qquad [6]$$

where INEPT and reverse INEPT refer to the refocused versions. In contrast to the sequence of Fig. 1c, this scheme has pronouncedly different effects for IS, I_2S, and I_3S spin systems. This is a result of the fact that this pulse scheme utilizes *refocused* INEPT schemes and that for I_2S and I_3S spin systems no complete refocusing of transverse magnetization can be obtained. This is illustrated below for the case of an I_2S system. The two protons are labeled I_1 and I_2. Immediately after the two simultaneous 90° (I, S) pulses of the INEPT transfer, two terms are created, $2I_{1z}S_y + 2I_{2z}S_y$. When each of these terms refocuses during the delay, 2τ, to form in-phase S-spin magnetization, they also defocus because of J coupling to the second spin. For example,

$$2I_{1z}S_y \xrightarrow{J_{NH}I_2 \cdot St} 2I_{1z}S_y \cos^2 \pi J_{IS}t - 4I_{1z}I_{2z}S_x \sin \pi J_{IS}t \cos \pi J_{NH}t$$
$$- 2I_{2z}S_y \sin^2 \pi J_{IS}t - S_x \sin \pi J_{IS}t \cos \pi J_{IS}t. \qquad [7]$$

This shows that the total in-phase S-spin magnetization, transferred from spin I_1, never becomes larger than $S_x \sin \pi J_{IS}t \cos \pi J_{IS}t$, which has a maximum of $S_x/2$, for $t = 1/(4J_{IS})$. As will be commented on below, only in-phase S-spin magnetization present during t_1 contributes to the resonance intensity in the correlation spectrum obtained with the scheme of Fig. 1d. Therefore, the sensitivity for I_2S and I_3S groups is lower by a factor of 2 and ~ 3, respectively, compared with the regular Overbodenhausen experiment of Fig. 1c.

As is clear from expression [7], at the beginning of the t_1 period (which corresponds to the start of the decoupling sequence) there will always remain antiphase terms of the type $S_y I_{1z}$ and $S_x I_{1z} I_{2z}$. These terms do not get destroyed by the compos-

ite pulse decoupling sequence; in fact, after an integral number of cycles of a good composite pulse cycle such as WALTZ-16 (31) or DIPSI (32) applied to the I spins, the I_{1z} and I_{2z} components of these terms are unchanged and no spherical randomization occurs (33). Neglecting I-spin offset effects, the remaining fraction of the last composite pulse cycle corresponds to a rotation of the I spins by an angle, β, that is the sum of the flip angles (including their sign) of the remaining fraction of the cycle. This summed angle, β, is a function of t_1 and affects the amount of magnetization that is transferred back from the antiphase terms to spin I. Since β is a function of t_1, with a very complex behavior, the transfer of antiphase S-spin magnetization back to spin I also follows this complex function, resulting after 2D FT in a pattern that looks like t_1 noise for the I_2S and I_3S resonances. A similar noise-like F_1 pattern is also obtained for IS groups if the refocusing delays, τ, are not set to $1/(4J_{IS})$. As explained below, this unwanted and spurious type of transfer, which also shows different relaxation characteristics, can be eliminated by the application of a 90° purge pulse (34) at the end of the composite pulse decoupling sequence. If all pulses of the composite decoupling cycle are applied along, for example, the x axis, the summed flip angle, β, is also applied along the x axis (neglecting offset effects). Therefore, the effect of this summed pulse on antiphase S-spin magnetization, S_yI_z is given by

$$S_yI_z \xrightarrow{\ \beta_x(I)\ } S_yI_z\cos\beta - S_yI_y\sin\beta. \qquad [8]$$

The subsequent $90°_y$ purge pulse converts these terms according to

$$S_yI_z\cos\beta - S_yI_y\sin\beta \xrightarrow{\ 90°_y(I)\ } S_yI_x\cos\beta - S_yI_y\sin\beta. \qquad [9]$$

Neither of the latter two terms is converted into observable ^1H magnetization by the subsequent reverse INEPT sequence, and therefore, the t_1-noise-like pattern is suppressed by this additional pulse.

RESULTS AND DISCUSSION

We have applied the techniques discussed above to two proteins, calmodulin ligated with Ca^{2+} and uniformly labeled with ^{15}N and staphylococcal nuclease (S. Nase), ligated with Ca^{2+} and 3′,5′-diphosphothymidine (pdTp). For both samples, the concentration was 1.5 mM; for calmodulin: 90% H_2O, pH 6.2, 47°C; for S. Nase: 99.9% D_2O, p^{2}H 7.4, 37°C.

FIG. 2. Comparison of ^{15}N–^1H correlation spectra, recorded with the schemes of Figs. 1a–1d, for the protein calmodulin. Spectra are recorded at 500 MHz ^1H frequency, 47°C, 1.5 mM, pH 6.2, 90% H_2O, 100 mM KCl, 6 mM Ca^{2+}. All spectra have been recorded with identical t_2 acquisition times (138 ms), and identical t_2 digital filtering (Lorentzian–Gaussian filter). No t_1 digital filtering was used. The acquisition times in the t_1 dimension were (a, b) 128 ms, (c) 165 ms, and (d) 240 ms. The F_2 digital resolution is 7 Hz (F_2) for all spectra. F_1 digital resolution is (a, b) 4 Hz and (c, d) 2 Hz. Spectra a–d have been recorded with the pulse schemes of Figs. 1a–1d. (a) Correlations that show resolved homonuclear J splittings in the F_1 dimension have been marked ▲. (b) Correlations that are severely attenuated upon presaturation (spectra a, c, d) are marked by arrows. (c) NH_2 correlations are marked by horizontal bars, connecting the two nonequivalent proton resonances. These resonances are absent in spectrum d.
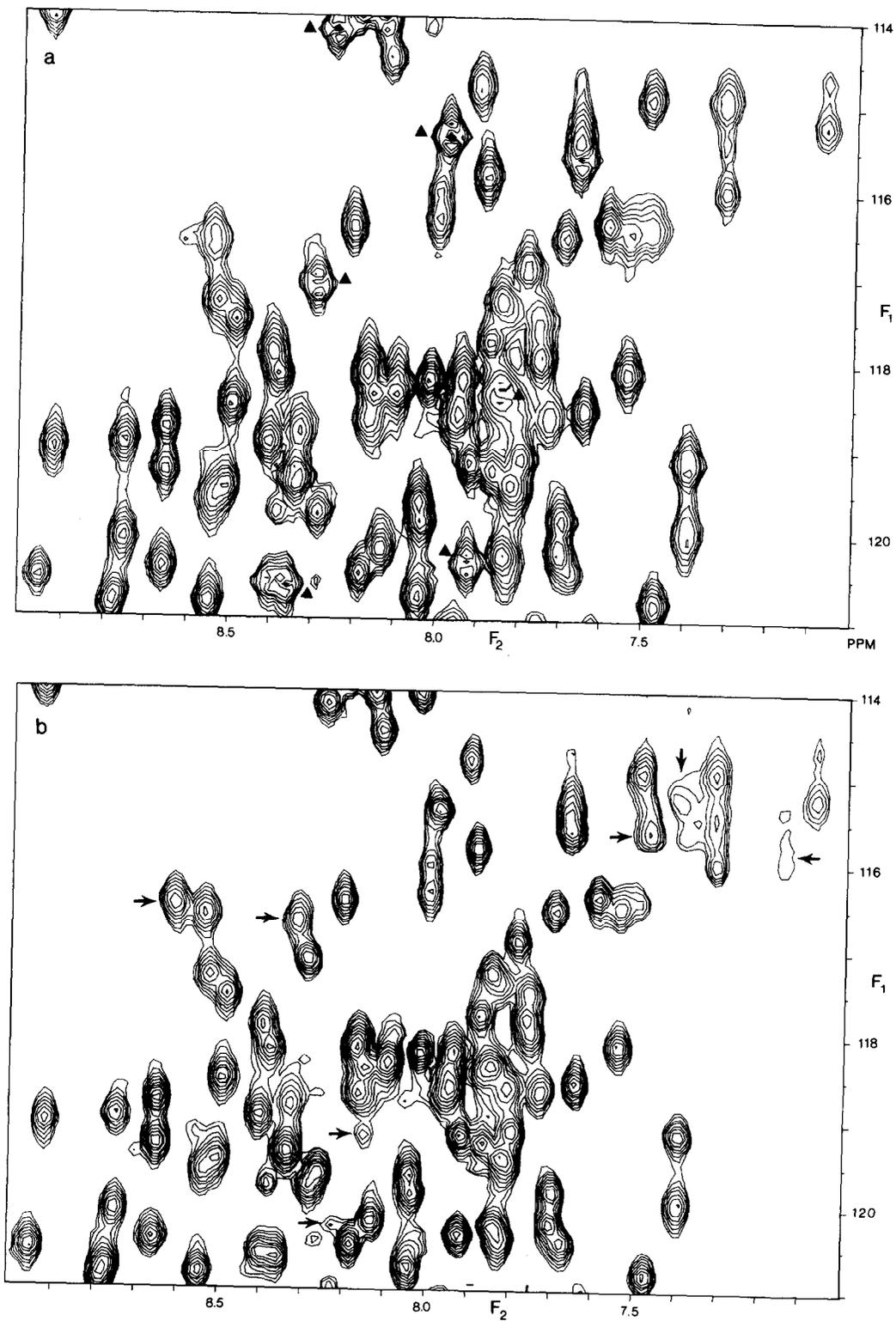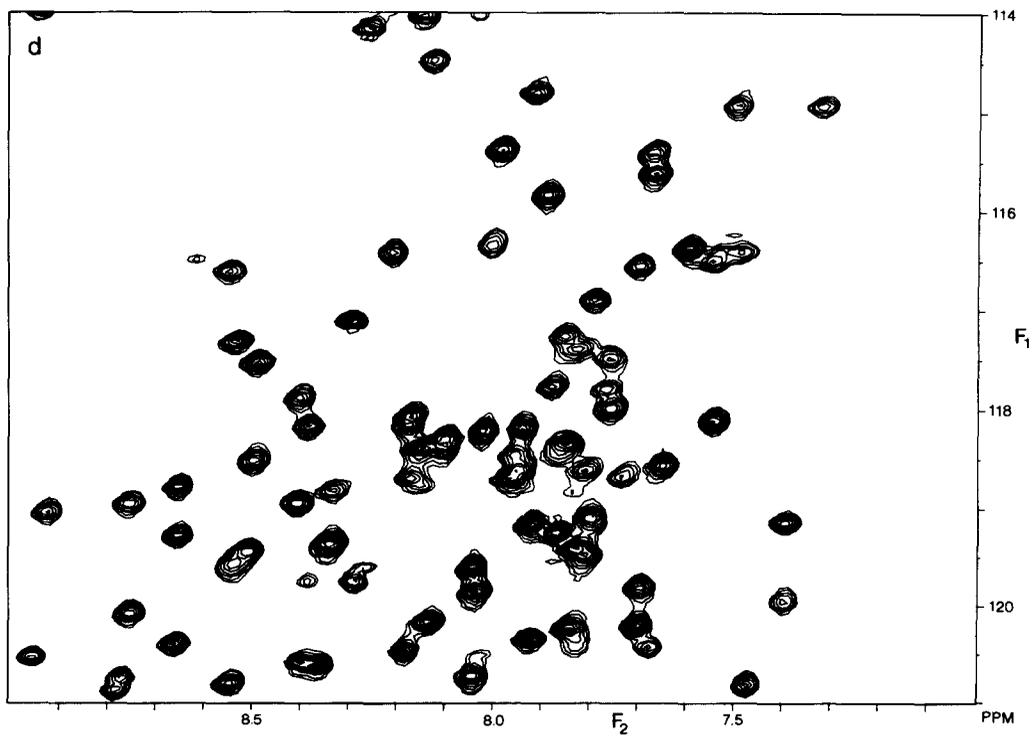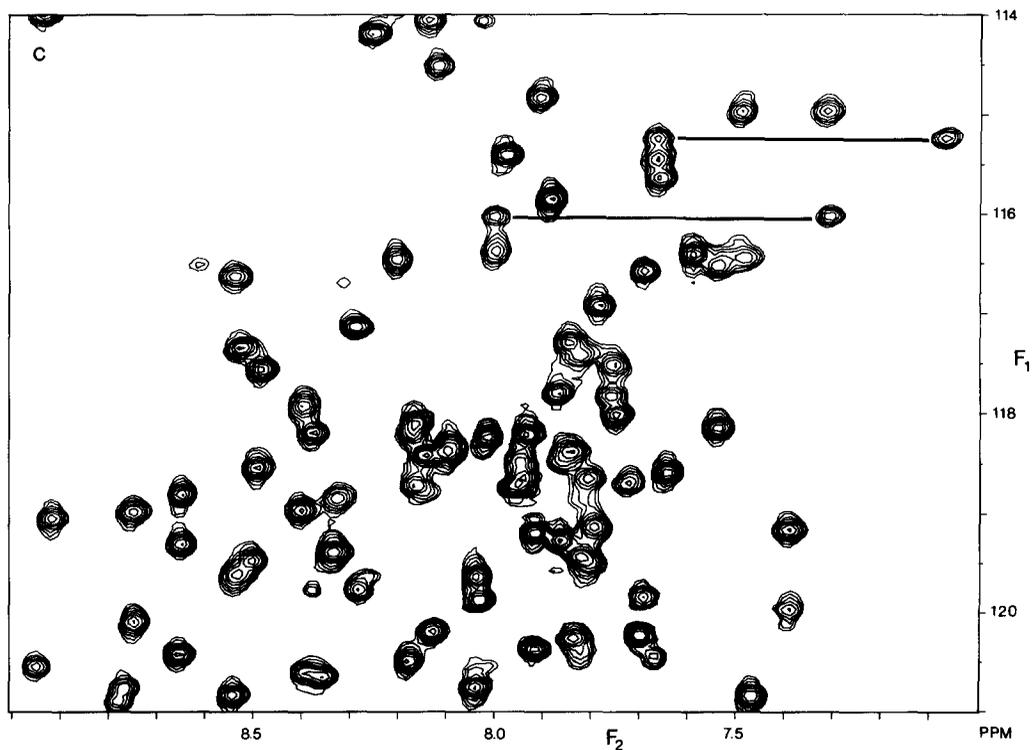
FIGURE 2

FIG. 2—*Continued*

^1H-^{15}N correlation. Figure 2 compares the results obtained with the four methods for a small region of the ^{15}N-^1H correlation map. The spectra in Figs. 2a–2d have been recorded with the pulse schemes of Figs. 1a–1d. No digital filtering has been used in the F_1 dimension; the same amount of Lorentzian-to-Gaussian digital filtering in the F_2 dimension was used for all four spectra. The t_2 acquisition time for all four experiments was 138 ms. The t_1 acquisition time was adjusted such that all signals had decayed by at least a factor 20; i.e., the t_1 acquisition was adjusted to be longer than $3 \times T_2$, where T_2 is the decay rate of the multiple-quantum coherence (Figs. 2a, 2b) or of the ^{15}N transverse magnetization (Figs. 2c, 2d). Thus, t_1 acquisition times were 128 ms (Figs. 2a, 2b), 165 ms (Fig. 2c), and 240 ms (Fig. 2d). For all spectra, the F_2 digital resolution is 7 Hz, and after zero filling, the F_1 digital resolution is 4 Hz (Figs. 2a, 2b) and 2 Hz (Figs. 2c, 2d).

Figure 2a shows the poorest F_1 resolution of the four spectra, mainly because of poorly or unresolved homonuclear J splittings in the F_1 dimension and the (antiphase) dispersive contributions associated with these J splittings. As discussed above, this phase distortion is a result of the homonuclear NH–CαH J coupling. Although this J coupling effect ruins the resolution of the correlation map, it also offers a unique opportunity to measure these important J couplings in a straightforward manner from such spectra (26). Figure 3 compares F_1 traces taken through the resonance of residue Asn-137, for each of the four spectra. The homonuclear J splitting is clearly visible in Fig. 3a, even without the use of any resolution enhancement. Note, however, that because of the antiphase dispersive contributions to this doublet, a small correction must be made to obtain the correct J coupling from the measured splitting (26).

The spectral region shown in Fig. 2b shows slightly better resolution than what is obtained with the scheme in Fig. 1a, largely because the correlations are now purely absorptive, and also because the remaining F_1 heteronuclear long-range ^{15}N-^1H J couplings are typically smaller than the homonuclear NH–CαH J coupling. This is illustrated by the F_1 section taken through the correlation of Asn-137 (Fig. 3b) which shows a single resonance, with a linewidth that is about 5 Hz larger than the width of an individual doublet component in Fig. 3a. This indicates that for this residue, the unresolved ^1H-^{15}N long-range couplings contribute 5 Hz to the F_1 linewidth.

A second major difference between Figs. 2a and 2b is that for the spectrum of Fig. 2b no presaturation of the H_2O resonance is used; i.e., even for amides whose protons exchange relatively rapidly with solvent (between 50 and 2 s^{-1}), NH correlations can be observed in Fig. 2b, whereas, because of H_2O presaturation, such correlations are severely attenuated in Figs. 2a, 2c, and 2d.

As can be seen in Figs. 2c, 2d, a significant increase in F_1 resolution is obtained with the schemes of Figs. 1c, 1d. As discussed above, the F_1 linewidth is now determined by the transverse relaxation rate of a ^1H-coupled ^{15}N resonance (Fig. 2c) and of the ^1H-decoupled ^{15}N resonance (Fig. 2d). Comparison of Figs. 2c and 2d indicates that the contribution from scalar relaxation of the second kind (which affects Fig. 2c and not 2d) is substantial. For the correlation of Asn-137, Figs. 3c and 3d indicate a difference of about 2 Hz, which is approximately 30% of the linewidth. Especially in Fig. 2d, small differences in the F_1 linewidth of the various correlations become apparent, probably reflecting some differences in local mobility. Complete resonance assign-
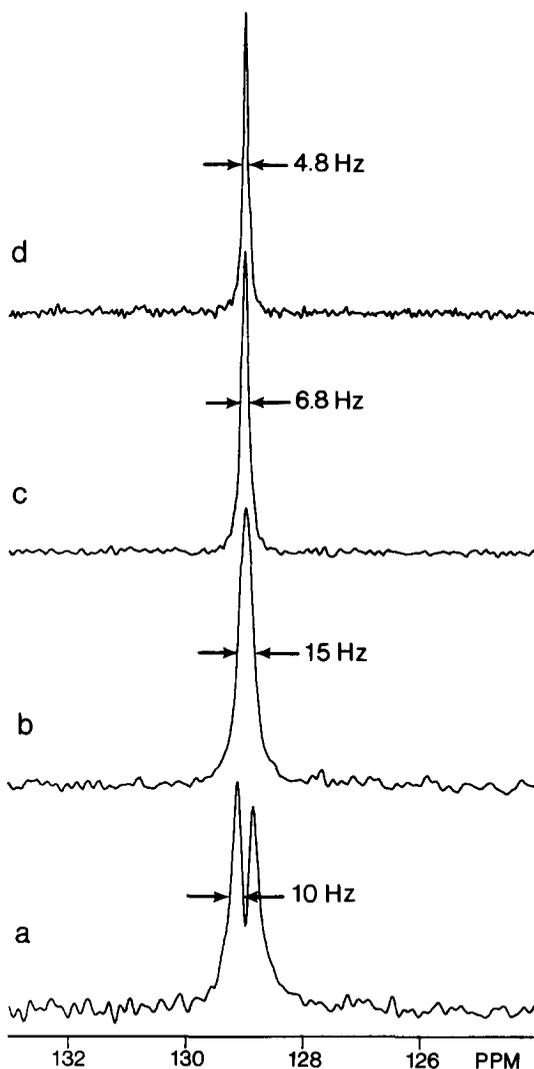
FIG. 3. (a–d) F_1 sections taken through the resonance of Asn-137 for the spectra shown in Figs. 2a–2d, recorded with the pulse schemes of Figs. 1a–1d. The digital resolution is 0.25 Hz; no F_1 filtering has been used. The J splitting observed in (a) is larger than the actual NH–CαH J coupling because of small anti-phase dispersive contributions of the two doublet components (26).

ments and a study of the local backbone dynamics of calmodulin and S. Nase are currently still in progress, and these results will be presented elsewhere.

As discussed above, the NH_2 resonances are suppressed by the pulse sequence of Fig. 1d, but not with the sequence of Fig. 1c. Comparison of Figs. 2c and 2d therefore immediately identifies the NH_2 correlations, in a manner analogous to the editing procedure described previously (35). The NH_2 resonances, originating from Asn and Gln amino acids, have been marked by horizontal bars in Fig. 2c. Often, weak correlations are observed adjacent to the NH_2 correlations, but shifted about 0.6 ppm
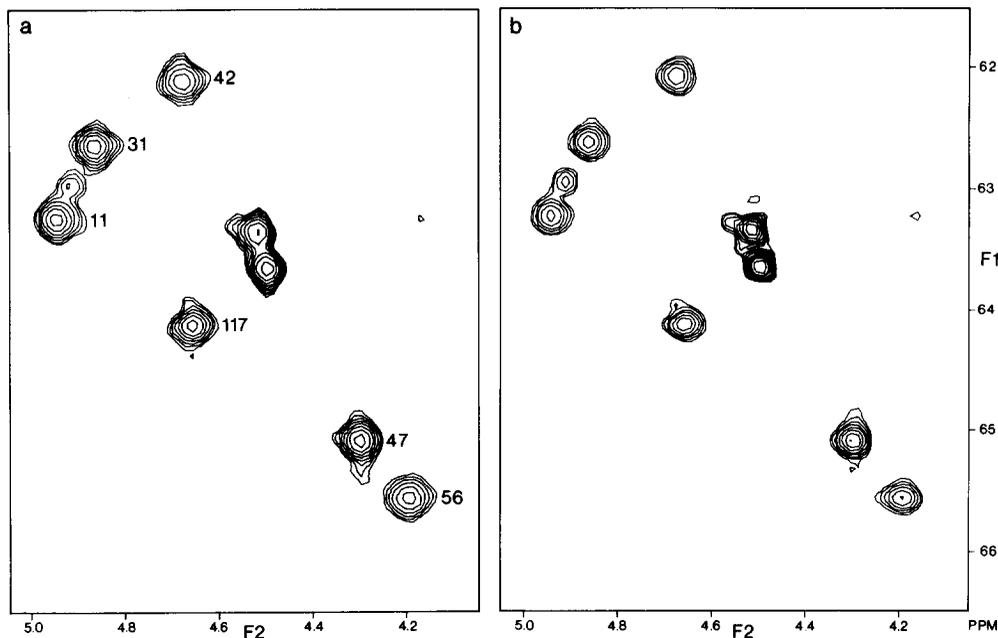
FIG. 4. Comparison of the ^1H–^{13}C correlation spectra recorded with the pulse schemes of Fig. 1a (a) and Fig. 1d (b), for the protein staphylococcal nuclease, containing $^{13}C\alpha$, ^{15}N-Pro. Spectra were recorded in 99.9% D_2O, 1.5 mM protein, 5 mM 3',5'-diphosphothymidine, 10 mM Ca^{2+}, p^2H 6.5. No filtering was used in the t_1 dimension; a Lorentzian-to-Gaussian transformation was used in the t_2 dimension for both spectra. The t_1 and t_2 acquisition times were 128 and 138 ms, respectively. The final digital resolution is 7 Hz (F_2) and 4 Hz (F_1). The number of transients per t_1 value was (a) 32 and (b) 160. Labels in (a) correspond to the residue number.

upfield in the ^{15}N dimension. These weak resonances originate from the semideuterated NHD moieties; the 0.6 ppm upfield shift reflects the deuterium isotope effect.

^1H–^{13}C correlation. In principle, there is no difference between ^1H–^{15}N and ^1H–^{13}C correlation. In practice, however, the substantial difference in heteronuclear dipolar coupling ($D_{CH}/D_{NH} \approx 2.1$) changes the relative importance of the heteronuclear dipolar coupling as a relaxation mechanism. Both for the ^1H attached to ^{13}C and for ^{13}C itself, the heteronuclear dipolar coupling is commonly the dominant relaxation mechanism. The fact that the heteronuclear dipolar coupling, to first order, does not contribute to the relaxation of the ^1H–^{13}C zero- and double-quantum coherence is therefore expected to have more impact for ^{13}C than for ^{15}N. To investigate this, we have recorded ^1H–^{13}C correlation spectra of S. Nase, labeled with ^{15}N, $^{13}C\alpha$-Pro.

Figures 4a and 4b show the ^1H–^{13}C correlation maps obtained with the sequences of Figs. 1a and 1d, respectively. The F_1 linewidth for the spectrum of Fig. 4a is determined by the multiple-quantum relaxation rate, superimposed on the (unresolved) $C\alpha^1H$ multiplet structure and the ^{15}N–^{13}C J coupling, which also are present in the F_1 dimension. Inspection of the F_1 trace taken through the $C\alpha$ resonance of Pro-56 (Fig. 5a) shows a linewidth of 29 Hz; approximately half of this width is attributed to ^1H–^1H J couplings and the unresolved ^{15}N–$^{13}C\alpha$ J coupling (≈ 6 Hz). The decou-
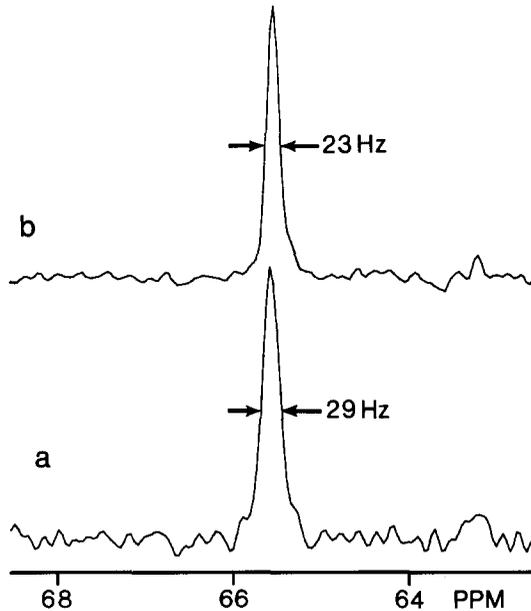
FIG. 5. Comparison of F_1 sections taken through the spectra of Fig. 4. Spectrum a was recorded with the sequence of Fig. 1a, and spectrum b was recorded with the scheme of Fig. 1d. The linewidth in spectrum a is determined by the T_2 of the $^{13}C^{-1}H$ multiple-quantum coherence and also by the (unresolved) $C\alpha H^{-}$ $C\beta H_2$ J couplings and the $^{15}N^{-13}C$ J coupling (≈ 6 Hz). The linewidth in spectrum b is determined by the ^{13}C T_2 and by the unresolved $^{15}N^{-13}C$ J coupling.

pled Overbodenhausen spectrum (Fig. 4b) shows slightly higher F_1 resolution, due in part to the absence of antiphase dispersive contributions, present in Fig. 4a. The F_1 trace taken through the correlation of Pro-56 shows a linewidth of 23 Hz, 6 Hz narrower than the multiple-quantum unresolved J multiplet of Fig. 5a.

CONCLUSIONS

We have shown that for proteins the resolution obtainable in $^1H^{-15}N$ shift correlation maps depends strongly on the pulse scheme used. The resolution of the multiple-quantum type correlation experiments suffers in comparison to the single-quantum correlation techniques, mainly because of the presence of often unresolved homonuclear or heteronuclear multiple-bond J couplings. Moreover, the true relaxation rate of the multiple-quantum coherence is commonly higher than the transverse relaxation rate of ^{15}N magnetization. This was the major consideration by Opella and co-workers for using the conventional ^{15}N-detected shift correlation experiment in their study of Pf1 filamentous bacteriophage coat protein (36). As shown here, the decoupled Overbodenhausen experiment also presents ^{15}N linewidths that are determined by the ^{15}N transverse relaxation rate, and which should be completely equivalent to the ^{15}N-detected counterparts, apart from an approximate 30-fold gain in sensitivity (18).

We have shown that the effect of scalar relaxation of the second kind on the ^{15}N linewidth of proteins in Overbodenhausen type correlation spectra is significant and

that this effect can be removed by using a synchronous composite pulse decoupling sequence during the evolution period. This decoupled Overbodenhausen experiment yields the highest possible resolution but it requires extra refocusing and defocusing delays, relative to the regular Overbodenhausen experiment. The choice of these delays affects the sensitivity of the correlation and the relative intensities of NH and NH_2 (or CH, CH_2, and CH_3), analogous to the intensities in a refocused INEPT experiment. A purge pulse is necessary at the end of the composite pulse decoupling scheme to avoid t_1-noise-like features in the 2D spectrum.

For ^{13}C, the obtainable resolution for the Overbodenhausen experiment is slightly higher than for the HMQC type experiment because, in the latter experiment, ^1H–^1H J coupling remains in the F_1 dimension. Although this coupling is usually unresolvable for larger proteins (>10 kDa), for smaller ^{13}C-labeled proteins this F_1 J splitting may make it possible to measure accurate ^1H–^1H J couplings from such correlations, as has been demonstrated recently for ^{15}N (37). For ^{13}C, the regular Overbodenhausen experiment is probably preferable over the decoupled version of the experiment because all moieties (CH, CH_2, and CH_3) appear with their full intensity. The fact that the regular experiment requires four fewer 180° pulses and does not require the relatively long refocusing/defocusing delays should also give it a small sensitivity advantage over the decoupled version.

REFERENCES

1. L. MÜLLER, J. Am. Chem. Soc. 101, 4481 (1979).
2. G. BODENHAUSEN AND D. J. RUBEN, Chem. Phys. Lett. 69, 185 (1980).
3. M. R. BENDALL, D. T. PEGG, AND D. M. DODDRELL, J. Magn. Reson. 52, 81 (1983).
4. A. BAX, R. H. GRIFFEY, AND B. L. HAWKINS, J. Magn. Reson. 55, 301 (1983).
5. A. G. REDFIELD, Chem. Phys. Lett. 96, 537 (1983).
6. S. ROY, M. Z. PAPASTAVROS, V. SANCHEZ, AND A. G. REDFIELD, Biochemistry 23, 4395 (1984).
7. L. MÜLLER, R. A. SCHIKSNIS, AND S. J. OPELLA, J. Magn. Reson. 66, 379 (1986).
8. A. A. MAUDSLEY, L. MÜLLER, AND R. R. ERNST, J. Magn. Reson. 28, 463 (1977).
9. G. BODENHAUSEN AND R. FREEMAN, J. Magn. Reson. 28, 471 (1977).
10. A. BAX AND G. A. MORRIS, J. Magn. Reson. 42, 501 (1981).
11. G. ORTIZ-POLO, R. KRISHNAMOORTI, J. L. MARKLEY, D. H. LIVE, D. G. DAVIS, AND D. COWBURN, J. Magn. Reson. 68, 303 (1986).
12. G. OTTING AND K. WÜTHRICH, J. Magn. Reson. 76, 569 (1988).
13. G. WAGNER AND D. BRUEWHILER, Biochemistry 25, 5839 (1986).
14. V. SKLENAR AND A. BAX, J. Magn. Reson. 71, 379 (1987).
15. J. GLUSCHKA AND D. COWBURN, J. Am. Chem. Soc. 109, 7879 (1987).
16. R. H. GRIFFEY AND A. G. REDFIELD, Q. Rev. Biophys. 19, 51 (1987).
17. D. A. TORCHIA, S. W. SPARKS, AND A. BAX, Biochemistry, in press.
18. A. BAX, in "Methods in Enzymology" (N. Oppenheimer and T. L. James, Eds.), Vol. 176, pp. 134–150, Academic Press, San Diego, 1989.
19. G. A. MORRIS AND R. FREEMAN, J. Am. Chem. Soc. 101, 760 (1979).
20. R. FREEMAN, private communication, 1981.

21. A. ABRAGAM, "The Principles of Nuclear Magnetism," p. 309, Clarendon Press, Oxford, 1961.
22. R. R. ERNST, G. BODENHAUSEN, AND A. WOKAUN, "Principles of Nuclear Magnetic Resonance in One and Two Dimensions," pp. 25–32, Clarendon Press, Oxford, 1987.
23. M. F. SUMMERS, L. G. MARZILLI, AND A. BAX, *J. Am. Chem. Soc.* **108,** 4285 (1986).
24. D. J. STATES, R. HABERKORN, AND D. J. RUBEN, *J. Magn. Reson.* **48,** 286 (1982).
25. D. MARION AND K. WÜTHRICH, *Biochem. Biophys. Res. Commun.* **113,** 967 (1983).
26. L. E. KAY AND A. BAX, *J. Magn. Reson.* **86,** 110 (1990).
27. A. BAX, L. E. KAY, S. W. SPARKS, AND D. A. TORCHIA, *J. Am. Chem. Soc.* **111,** 408 (1989).
28. V. SKLENAR AND A. BAX, *J. Magn. Reson.* **74,** 469 (1987).
29. D. P. BURUM AND R. R. ERNST, *J. Magn. Reson.* **39,** 163 (1980).
30. P. H. BOLTON, *J. Magn. Reson.* **41,** 287 (1980).
31. A. J. SHAKA, J. KEELER, AND R. FREEMAN, *J. Magn. Reson.* **53,** 313 (1983).
32. A. J. SHAKA, C. J. LEE, AND A. PINES, *J. Magn. Reson.* **77,** 274 (1988).
33. M. H. LEVITT, G. BODENHAUSEN, AND R. R. ERNST, *J. Magn. Reson.* **55,** 443 (1983).
34. O. W. SØRENSEN AND R. R. ERNST, *J. Magn. Reson.* **51,** 477 (1983).
35. L. E. KAY AND A. BAX, *J. Magn. Reson.* **84,** 598 (1989).
36. R. A. SCHIKSNIS, M. J. BOGUSKY, P. TSANG, AND S. J. OPELLA, *Biochemistry* **26,** 1373 (1987).
37. L. E. KAY, B. BROOKS, D. A. TORCHIA, S. W. SPARKS, AND A. BAX, *J. Am. Chem. Soc.* **111,** 5488 (1989).
38. J. CAVANAGH AND J. KEELER, *J. Magn. Reson.* **78,** 186 (1988).